Spectroscopy and Kerr-lens mode-locked operation of Yb:GdScO3 crystal

Longxin Liu, Siyuan Niu, Zhiyong Liang, Zhenxin Jiang, Qingsong Song, Zebin Wang, Peng Chen, Jian Liu, Wenlong Tian, Jie Ma, et al.

Research Article Vol. 32, No. 9 / 22 Apr 2024 / Optics Express 16065
Optics EXPRESS

Spectroscopy and Kerr-lens mode-locked operation of Yb:$GdScO_3$ crystal

Longxin Liu,[1] Siyuan Niu,[2] Zhiyong Liang,[1] Zhenxin Jiang,[1] Qingsong Song,[3] Zebin Wang,[1] Peng Chen,[1] Jian Liu,[1,5] Wenlong Tian,[2] Jie Ma,[1] Xiaodong Xu,[1,6] Kheirreddine Lebbou,[4] and Jun Xu[3]

[1]*Jiangsu Key Laboratory of Advanced Laser Materials and Devices, School of Physics and Electronic Engineering, Jiangsu Normal University, Xuzhou 221116, China*
[2]*School of Optoelectronic Engineering, Xidian University, Xi'an 710071, China*
[3]*School of Physics Science and Engineering, Institute for Advanced Study, Tongji University, Shanghai 200092, China*
[4]*Institut Lumière Matière, UMR5306 Université Lyon1-CNRS, Université de Lyon, Lyon 69622, Villeurbanne Cedex, France*
[5]*jianliu586@jsnu.edu.cn*
[6]*xdxu79@jsnu.edu.cn*

Abstract: A Kerr-lens mode-locked laser based on a Yb^{3+}-doped disordered gadolinium scandate (Yb:$GdScO_3$) crystal is reported for the first time, to the best of our knowledge. The crystal with the perovskite structure was grown using the Czochralski method, and its room temperature (RT) and low temperature (LT) spectra were also investigated. Due to the crystal's multisite structure (Gd^{3+}/Sc^{3+} site), Yb:$GdScO_3$ offers broad and intense polarized emission spectra in the near-infrared range (975–1075 nm). The stimulated emission cross section σ_{SE} is 0.46×10^{-20} cm^2 at 1000 nm with an emission band width of 75.7 nm for E // b polarization. The continuous wave (CW) laser was operated pumped by a 976 nm fiber-coupled LD laser, resulting in a maximum output power of 8.74 W with a slope efficiency of 76.1% was obtained. Additionally, a pulses as short as 74 fs are generated at ~1061.7 nm via Kerr-lens mode-locking. The average output power amounts to 32 mW at a pulse repetition rate of 101.4 MHz. All results indicate Yb:$GdScO_3$ a promising candidate for 1 μm ultrashort laser.

1. Introduction

1 μm lasers have significant applications in high-power pump sources, laser radar, and medical and scientific research [1–4]. Yb^{3+} ions, with only two energy levels and short energy spacing, offer advantages over Nd^{3+} doped crystals by avoiding parasitic effects like excited-state absorption, energy-transfer upconversion, and cross-relaxation [5,6]. The low quantum defect (~7%) resulting from the in-band pumping scheme enhances laser efficiencies and reduces thermal load. Furthermore, the wider emission bandwidth and longer fluorescence lifetime [7] support ultra-strong, ultra-short pulse generation. Yb-based femtosecond lasers capable of delivering sub-100 fs pulses have been demonstrated in various crystals, such as Yb:$Y_3Al_5O_{12}$ (35 fs) [8], Yb:Lu_2O_3 (35 fs) [9], Yb:YSO (95 fs) [10], Yb:$CaYAlO_4$ (17 fs) [11], Yb:$YAlO_3$ (29 fs) [12], and Yb:$SrLaAlO_4$ (30 fs) [13]. Host materials with smooth and broadband emission spectra, along with good mechanical, thermal, and optical properties, play a crucial role in further shortening the pulse duration.

$GdScO_3$ crystal has an orthorhombic perovskite structure with the space group *Pnma* (No. 62) [14]. Known for its low phonon energy (~452 cm^{-1}) and high thermal stability [15], $GdScO_3$ crystals have garnered significant attention in the advancement of solid-state lasers. For instance, Er:$GdScO_3$ crystals grown using the edge-defined film-fed (EFG) method have demonstrated

#521962 https://doi.org/10.1364/OE.521962
Journal © 2024 Received 20 Feb 2024; revised 28 Mar 2024; accepted 29 Mar 2024; published 16 Apr 2024

Optics EXPRESS

impressive results, achieving a high power continuous wave (CW) laser output of 0.863 W at approximately 2700 nm with a slope efficiency of 11.25% [16]. Tm:$GdScO_3$ crystals have shown tunable laser operation at 321 nm and produced pulses as short as 44 fs [17,18]. Additionally, $GdScO_3$ has proven to be a versatile host material for lasers operating in the 1 µm, 2 µm, and 3 µm regions. Notably, Nd:$GdScO_3$ crystals have achieved a maximum output power of 3.16 W with a slope efficiency of 47.5% [19], while Yb:$GdScO_3$ crystals have generated a maximum output power of 13.45 W with an optical-to-optical efficiency of 63.3% [20]. The broad emission bandwidth of 85 nm suggests the potential for ultrashort pulse lasers. However, no advancements in pulse laser technology have been reported yet. Therefore, further research is crucial to fully explore the capabilities of $GdScO_3$ crystals in ultrafast laser applications.

In this research, a Yb^{3+} doped $GdScO_3$ crystal has been grown by the Czochralski method. The polarized absorption and emission spectra of the Yb:$GdScO_3$ crystal were analyzed at both room temperature and low temperature (77 K). Additionally, the laser performance was analyzed in both continuous wave (CW) and Kerr-lens mode-locked regimes. The Yb:GdScO3 laser was able to generate soliton pulses as short as 74 fs at 1061.7 nm, operating at a frequency of approximately 101.4 MHz.

2. Crystal growth and structure

The Yb:$GdScO_3$ crystal was grown using the Czochralski method. The Yb_2O_3, Gd_2O_3, and Sc_2O_3 powders with the purity of 5N were prepared as raw materials and weighed according to the formula: $Yb_{0.04}Gd_{0.96}ScO_3$. The mixed powders were pressed into bulks and then sintered in the air at 1400°C for 24 h. The treated blocks were then positioned within iridium crucibles under a nitrogen atmosphere for crystal growth. The single-crystal growth process comprises three principal steps: shoulder release, equalizing, and closing. The pulling speed for this process varies between 0.5 and 1.5 mm/h, with the rotational speed around to 15 rpm. High-purity nitrogen gas was introduced as a protective atmosphere during the crystal growth. The crystals were cooled to room temperature at a rate of 40 °C/h. The photograph of as-grown 4 at.% Yb:$GdScO_3$ crystal is shown in Fig. 1.

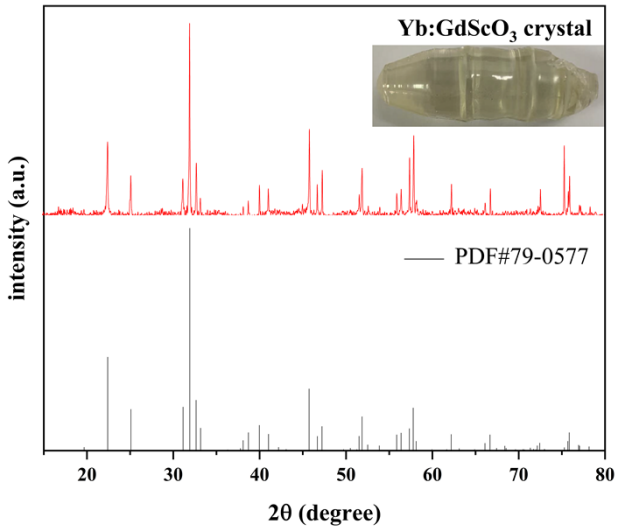

Fig. 1. The XRD patterns of Yb:$GdScO_3$ single crystal. The inset presents photograph of the as-grown Yb:$GdScO_3$ bulk.

Optics EXPRESS

Figure 1 displays the XRD patterns of 4 at.% Yb:$GdScO_3$ crystals compared to the standard card of $GdScO_3$ crystal (PDF#27-0220). The diffraction peaks of Yb:$GdScO_3$ crystals align well with the $GdScO_3$ phase, indicating a shared crystal structure. Calculated lattice parameters for Yb:$GdScO_3$ crystal are a = 0.5434 nm, b = 0.5724 nm, and c = 0.7911 nm, slightly smaller than those of pure $GdScO_3$ (a = 0.5487 nm, b = 0.5756 nm, and c = 0.7926 nm) [21]. This reduction in lattice parameters is attributed to the substitution of Yb^{3+} with a smaller cation radius in place of Gd^{3+}.

3. Spectroscopic properties of Yb:$GdScO_3$

To determine the Stark splitting of the ground state and the excited-state of Yb^{3+} ions in $GdScO_3$, we have measured the low temperature (77 k) absorption and emission spectra for $E // a$, $E // b$, and $E // c$. In Fig. 2(a), At the low temperature (77K) absorption spectrum shows a prominent peak at 985.0 nm (10142 cm^{-1}), corresponding to the transition between the lowest Stark sub-levels of the $0 \rightarrow 0'$ multiplets (zero-phonon line). In cases where the structural symmetry is less than cubic, the ground state $^2F_{7/2}$ and excited state $^2F_{5/2}$ of Yb^{3+} split into four and three Stark levels, respectively. The peaks at 10,460 and 10,834 cm^{-1} are associated with the $0 \rightarrow 1'$ and $0 \rightarrow 2'$ transitions, respectively. At lower temperatures, the splitting peaks for different polarization directions are more distinct, nearly identical, and easily distinguishable.

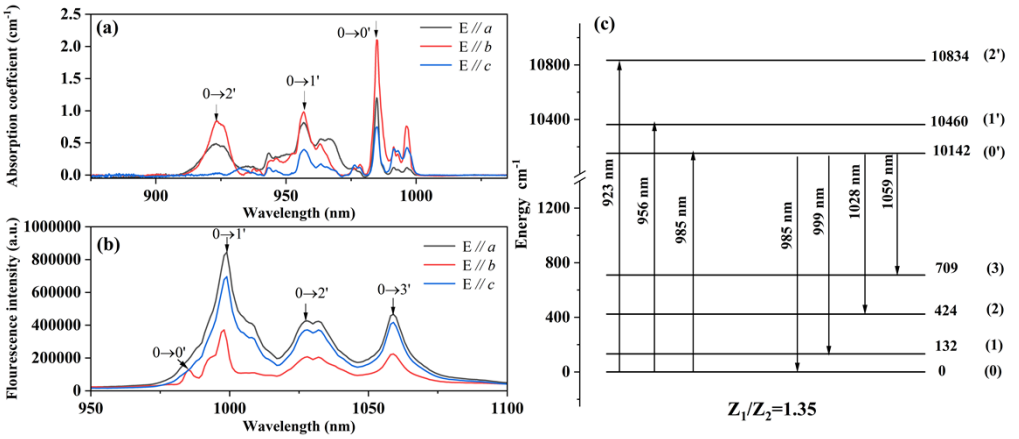

Fig. 2. Low-temperature polarized spectroscopy of the Yb:$GdScO_3$ crystal: (a) absorption and (b) luminescence spectra. (c) Energy-level diagram of Yb^{3+} in $GdScO_3$ crystal. $Z_{1(2)}$ are the partition functions.

The energy level diagram of Yb^{3+} ions in $GdScO_3$ was plotted based on the assignment of electronic transitions, and shown in Fig. 2(c). The ground-state exhibits a total splitting of 709 cm^{-1}, which is conducive to wavelength-tunable laser operations. In addition, Fig. 2(c) also presents the calculated partition functions $Z_{1(2)}$, for the ratio of Z_1/Z_2 1.35.

The Yb^{3+} concentration in the initial head region of the as-grown crystal was found to be 1.6 at.% through inductively coupled plasma atomic emission spectroscopy (ICP-AES). Subsequently, the effective segregation coefficient of Yb^{3+} in the $GdScO_3$ crystal can be determined as $k_{eff} = C_s/C_0 = 0.4$. The room temperature polarized absorption cross section of the Yb:$GdScO_3$ crystal is illustrated in Fig. 3(a). The results reveal that the absorption spectra display polarization-specific characteristics, with distinct absorption coefficients in each orientation. The absorption cross section of Yb^{3+} is computed using the formula [18]: $\sigma_{abs} = \alpha/N_0$ (where the corresponding Yb^{3+} ion densities are 2.25×10^{20} cm^{-3}). It is evident that the absorption line shapes for $E // a$ and $E // b$ are quite similar, but notably different from that for $E // c$. The most intense

Optics EXPRESS

absorption is observed at 985 nm for $E \,//\, b$, corresponding to the transition of $^2F_{7/2} \rightarrow {}^2F_{5/2}$, with a maximum absorption cross-section of 5.82×10^{-20} cm^2. The full width at half maximum (FWHM) is 19.7 nm, indicating that this material is suitable for pumping with commercial high-power InGaAs diode lasers for power scalable operation.

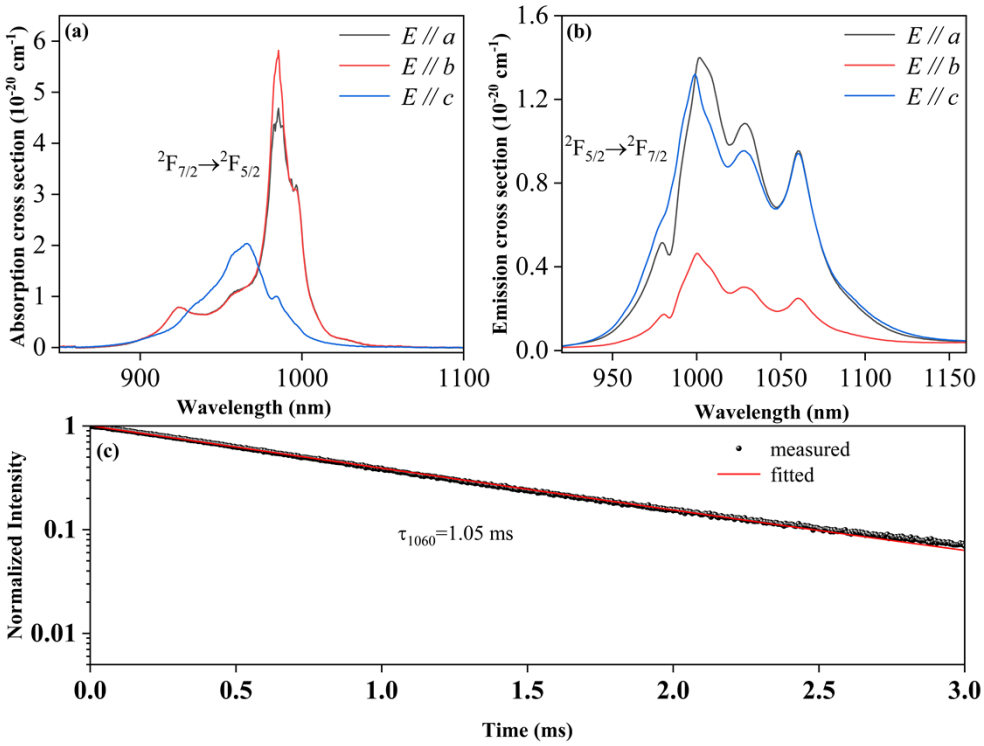

Fig. 3. The room temperature polarized (a) absorption cross section, (b) emission cross section versus wavelength, and (c) fluorescence decay curves of the $^2F_{5/2}$ multiplet of Yb:$GdScO_3$ crystal.

The RT stimulated-emission (SE) cross-sections, σ_{SE}, were calculated using a combination of the reciprocity method (RM) [22] and the Füchtbauer–Ladenburg (F-L) equation [23].

$$\sigma^i_{em}(\lambda) = \sigma^i_{abs}(\lambda)\frac{Z_1}{Z_2}exp\left(\frac{E_{ZL-hc/\lambda}}{kT}\right) \tag{1}$$

$$\sigma^i_{em} = \frac{\lambda^5}{8\pi n^2 c\tau}\frac{I_i(\lambda)}{\sum_{i=a,b,c}\int \lambda I_i(\lambda)d\lambda} \tag{2}$$

where the $\sigma^i{}_{abs}(\lambda)$ is the absorption cross section for the i polarization, k is the Boltzmann's constant, h is the Planck constant, E_{ZL} is the zero-line energy, Z_1 and Z_2 are partition functions for lower and upper levels.

For each polarization, represented by the variable i, with values a, b, or c, λ denotes the light wavelength, $I_i(\lambda)$ represents the measured emission spectrum, n represents the average refractive index, and τ signifies the radiative lifetime of the emitting state ($^2F_{5/2}$), which was determined to be 0.85 ms by using a modified reciprocity method.

The emission cross sections of $E \,//\, a$, $E \,//\, b$ and $E \,//\, c$ calculated by the FL method are 1002 nm 1.40×10^{-20} cm^2, 1000 nm 0.46×10^{-20} cm^2 and 1000 nm 1.30×10^{-20} cm^2, and the FWHMs are 79.5 nm, 75.7 nm, and 87.4 nm, respectively. Notably, Yb:$GdScO_3$ exhibits a wide emission

Optics EXPRESS

bandwidth in different polarization directions, which is higher than most well-studied materials, as shown in Table 1. Consequently, Yb:$GdScO_3$ demonstrates potential use for generating a broad tuning range laser and ultrafast mode-locked laser pulses.

Table 1. Comparison of the main spectral parameters of different Yb-doped crystals

Crystal	λ_{em} (nm)	σ_{em} (10^{-20}cm^2)	FWHM (nm)	τ_f (ms)	References
CaF_2	1049	0.17	70	2.4	[24]
$Y_3Al_5O_{12}$	1032	2.10	10	0.95	[25]
$YAlO_3$	1013	1.20	40	0.72	[25]
$CaYAlO_4$	1035	0.50	61	0.42	[26]
$LuScO_3$	1039	0.9	22	-	[27,28]
$YScO_3$	1037	0.21	-	0.87	[29]
$GdScO_3$	1002 (E // a)	1.4	79.5	1.05	This work
	1000 (E // b)	0.46	75.7		
	1000 (E // c)	1.3	87		

The gain characteristics of a laser can be characterized by the gain cross section of the laser crystal, which is given by the expression:$\sigma_g(\lambda) = \beta\sigma_{em}(\lambda) - (1-\beta)\sigma_{abs}(\lambda)$. β represents the proportion of inverted ions to the total Yb^{3+}-ion density. The polarized σ_{gain} spectra of 1000 ~ 1200 nm with different β values are shown in Fig. 4. In the case of a constant β, the generation of large laser gain is attributed to a larger emission cross section and a smaller self-absorption effect. The maximum σ_{gain} value (0.295×10^{-20} cm^2 at 1061 nm when $\beta = 0.32$) corresponds to light polarization E // c, similar to the value of E // a (0.291×10^{-20} cm^2 at 1060 nm). For both low β value and higher β value, the local peak centered at ~ 1060 nm dominates in the spectra for the three polarization. Compared to the other polarizations, the bandwidth of the E // c polarization is the largest at $\beta = 0.32$, which is close to 80 nm, while the gain bandwidths of the E // b and E // c polarizations are 59 nm and 39.8 nm, respectively. Such a large, broad, and flat profile of the gain cross section supports a wide band tunable and ultrashort pulse laser for Yb:$GdScO_3$ crystal. The experimental results indicate that Yb:$GdScO_3$ exhibits a broad and very flat gain spectrum in all three polarization cases.

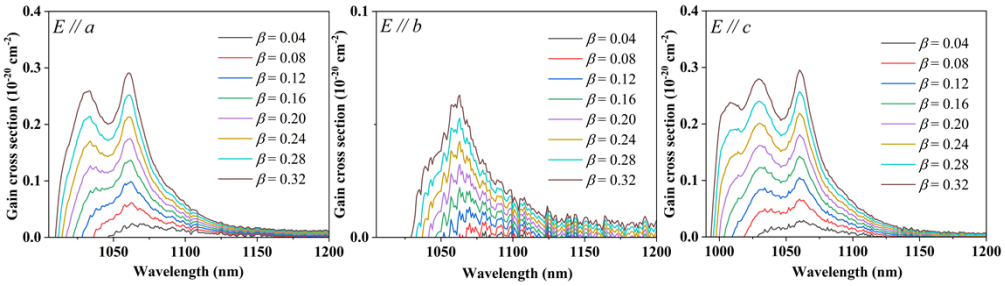

Fig. 4. Yb:$GdScO_3$ gain cross-section spectra at different ratios of inverted particle numbers β.

4. Laser set-up and continuous-wave (CW) operation

Firstly, we investigated the CW laser performance of the 3.5 mm-thick Yb:$GdScO_3$ crystal, and the setup depicted in Fig. 5(a). A compact two-mirror laser resonant cavity for CW laser performance was employed in this work, where the pump source was a fiber-coupled 976 nm InGaAs diode

Optics EXPRESS

laser with a core diameter of about 105 µm. After passing through a collimated lens ($f = 50$ mm) and a focused lens ($f = 75$ mm), the pump beam is focused onto the gain medium resulting in a spot size of about 157.5 µm. Initially, three different orientations (*a*-cut, *b*-cut, and *c*-cut)of Yb:$GdScO_3$ were tested under an pump power of 10.28 W, resulting in output powers of 2.05 W, 1.15 W, and 1.06 W, respectively, using a 5% output coupler transmission (T_{OC}). Subsequently, four different output couplers with varying transmission rates ($T_{OC} = 5\%$, 10%, 15%, and 20%) were employed to enhance the slope efficiency of the *a*-cut orientation. Eventually, the highest output power 8.74 W with a slope efficiency of 76.1% was achieved for $T_{OC} = 20\%$, as depicted in Fig. 5(b). The high slope efficiency is comparable to that of Yb:CLNGG (74%, [30]) and Yb:YLuGdCOB (70%, [31]), slightly lower than that of Yb:YSGG (80.1%, [32]) and Yb:CYA (92%, [7]), indicating the high quality of the Yb:$GdScO_3$ crystal.

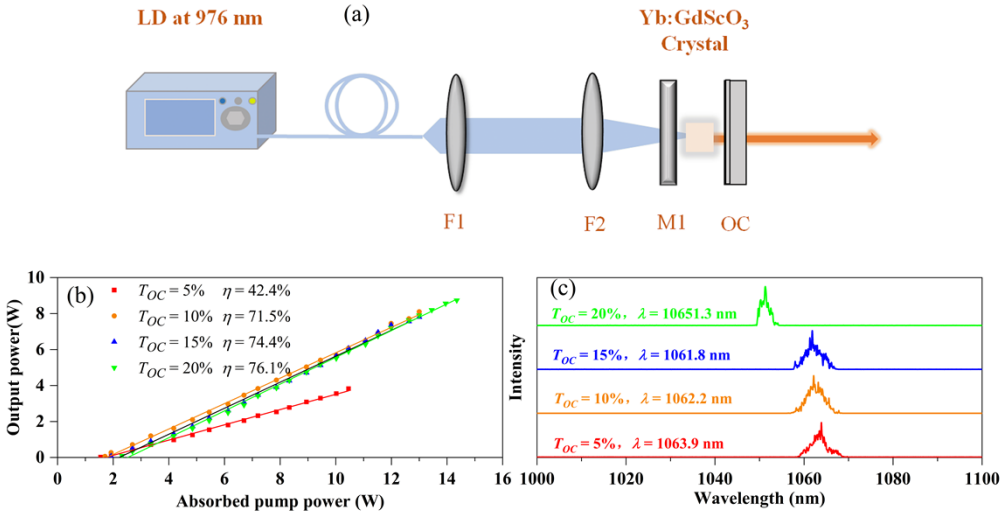

Fig. 5. (a) Scheme of the LD-pumped CW Yb:$GdScO_3$ laser; (b) Output power versus absorbed pump power of *a-cut* samples; (c) Laser emission spectra of *a-cut* at different OCs.

The corresponding laser spectra with different OCs are shown in Fig. 5(c). With the change of output couplers from $T_{OC} = 5\%$ to 20%, the cavity loss and the threshold become higher. In order to meet the requirements of laser oscillation, the beta value should be continuously increased, causing the maximum wavelength of $\sigma_g(\lambda)$ to move towards the short end. Consequently, the spectral peak demonstrates a blue shift as the OC reflectance increases in varying directions.

5. Mode-locked soliton laser operation

Figure 6 shows a schematic of the Kerr-lens mode-locked (KLM) laser setup with a standard Z-fold cavity. A $E // b$ Brewster angle-cut sample was mounted on a copper block heat sink with both end faces of the sample laser-graded polished, and a half-wave plate (HWP) was used to adjust the polarization of the incident pump for optimal absorption. The copper block heat sink was maintained at ~14.0°C by circulating water to remove heat generated during laser operation. The pump source is a commercial single mode fiber laser (ALS-IR-75, Azur Light Systems), emitting at 979 nm ($M^2 \sim 1.25$) with beam diameter 27 µm and up to 10 W output power. A collimated defocusing system consisting of a concave lens (*L1*) with a focal length of 25 mm and a convex lens (*L2*) with a focal length of 200 mm is used for recollimation. The pump beam is then focused into the crystal through a convex lens (*L3*) with a focal length of 75 mm. M4 and M5 were dichroic concave mirrors with 75 mm radium of curvature (R_{OC}), coated with high reflectivity over 1020-1100 nm ($R > 99.9\%$), and high transmittance around 800-1000 nm

Optics EXPRESS

($R < 5\%$). The optical dispersion was mitigated by employing diverse arrays of Gires-Tournois interferometer mirrors (GTIs) within the cavity, yielding a comprehensive group delay dispersion (GDD) ranging from -250 fs^2 to -1000 fs^2. And no extra-cavity pulse compression was employed. The total cavity length was about 1.5 m, corresponding to a repetition rate of 100 MHz.

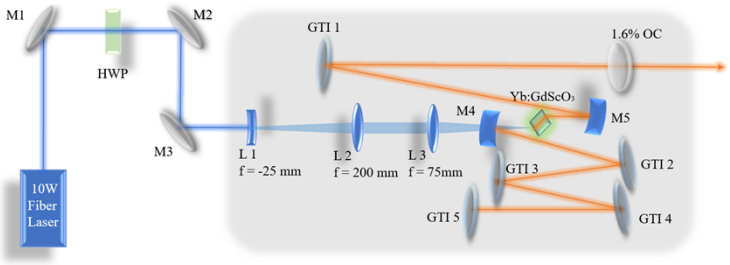

Fig. 6. Experimental setup of the KLM Yb:$GdScO_3$ laser. HWP: half wave plate; *L1*: concave lens, $f = 25$ mm; *L2*: convex lens, $f = 200$ mm; *L3*: convex lens, $f = 75$ mm; M4 and M5: concave mirrors with radius of curvature (R_{OC}) of 75 mm; GTI1-GTI5: Gires-Tournois interferometer mirrors; OC: optical coupler.

The KLM operation of the Yb:$GdScO_3$ laser was initially explored by employing an output coupler with a transmission of $T_{OC} = 0.4\%$ to minimize intracavity losses and generate ultrashort pulses. Manipulation of the KLM operation was achieved by slightly misaligning the M5 mirror, thus bringing the cavity closer to the periphery of the stability range. Using a commercial optical spectrum analyzer (AvaSpec-ULS2048, Avantes), the mode-locked optical spectrum was measured as shown in Fig. 7(a). The laser's optical spectrum, with a full width at half-maximum (FWHM) of 12.5 nm, exhibited a $sech^2$-shaped profile centered at 1059 nm. The corresponding intensity autocorrelation trace was measured by a commercial intensity auto-correlator (APE Pulse Check USB), as shown in Fig. 7(b). The recorded second-harmonic generation (SHG)-based intensity autocorrelation trace was well-represented by a $sech^2$-shaped temporal profile, estimating a pulse duration of 125 fs.

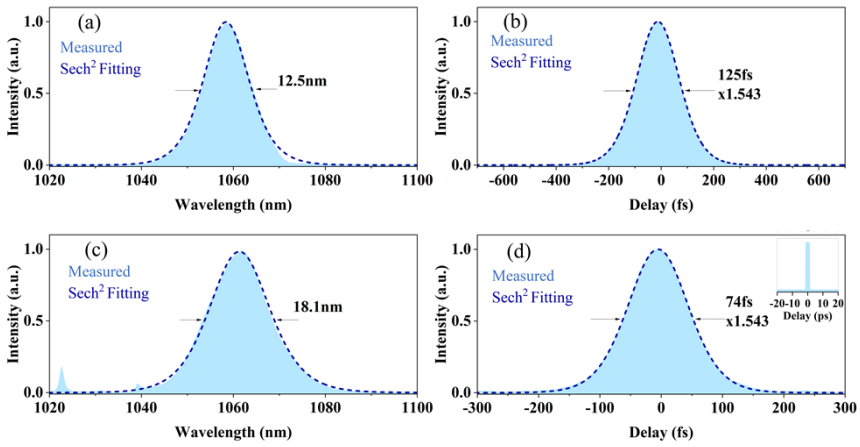

Fig. 7. (a) KLM Yb:$GdScO_3$ laser with $T_{OC} = 0.4\%$ Laser spectra; (b) SHG-based intensity autocorrelation trace; (c) KLM Yb:$GdScO_3$ laser with $T_{OC} = 1.6\%$ Laser spectrum; (d) SHG-based intensity autocorrelation trace. Inset: intensity autocorrelation trace measured on a time span of 40 ps.

Optics EXPRESS

Further reduction in pulse duration was accomplished by employing an output coupling of 1.6%. The Yb:$GdScO_3$ laser produced pulses with a spectral bandwidth of 18.1 nm at a center wavelength of 1061.7 nm (assuming a $sech^2$-shaped profile), as presented in Fig. 7(c). The fit of the recorded intensity autocorrelation trace with a $sech^2$-shaped temporal profile yielded an estimated pulse duration of 74 fs, with an average of 37 mW, observed in Fig. 7(d). The time bandwidth product of the laser is 0.35 which is close to the value of 0.315 for the transform limited $sech^2$-pulse, indicating the theoretically shortest pulse of 65.4 fs under the current conditions. The long-scale autocorrelation scan extending over 40 ps, depicted in the inset of Fig. 7(d), confirmed the operation of the laser in continuous-wave mode with mode-locked characteristics, devoid of any pedestals or multi-pulsing instabilities.

To ascertain the stability of the mode-locking operation, we conducted an analysis of the radio frequency (RF) spectrum using a commercial RF spectrum analyzer (Agilent 4407B). The signals were acquired within a frequency window of 0.2 MHz, utilizing a resolution bandwidth (RBW) of 100 Hz, and a frequency span of 0.9 GHz with a 1 kHz RBW, as illustrated in Figs. 8(a) and 8(b). The RF spectrum of the fundamental harmonic at 101.4 MHz exhibited a signal-to-noise ratio (SNR) of approximately 65 dBc. The absence of discernible side peaks in the higher-order harmonics suggests that the KLM operation remained stable, devoid of Q-switch instability. The observed fluctuations in the harmonic peaks within Fig. 8(b) may be attributed to the constrained sampling rate of the RF spectrum analyzer.

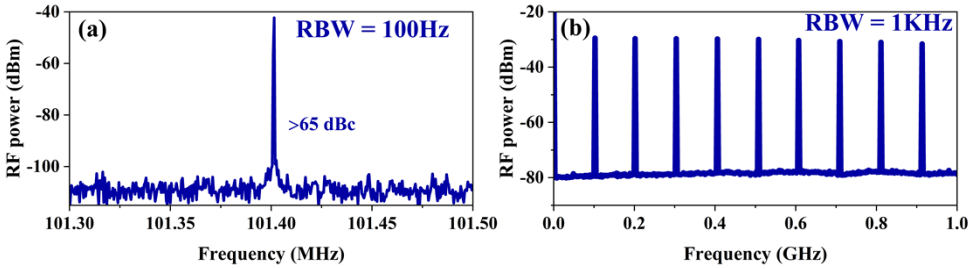

Fig. 8. Radio frequency (RF) spectra at: (a) the fundamental beat note with the resolution bandwidth (RBW) of 100 Hz, and (b) 0.9 GHz wide span range with 1 kHz RBW.

6. Conclusion

In summary, a Yb:$GdScO_3$ crystal with high-quality was successfully grown using the Czochralski method. To the best of our knowledge, the low-temperature spectral performance was investigated for the first time. For $E // b$ polarization, the maximum absorption cross section was determined to be 5.82×10^{-20} cm^2 at 985 nm. The stimulated emission cross section at 1000 nm was calculated to be 0.46×10^{-20} cm^2 with FWHM of 75.7 nm. Utilizing a 976 nm fiber laser as a pump source, a maximum output power of 8.74 W, accompanied by a slope efficiency as high as 76.1% was achieved. By using a mode-locking technique, the Yb:$GdScO_3$ laser produces soliton pulses as short as 74 fs at 1061.7 nm with an operating frequency of ~101.4 MHz. Through further appropriately managing the intracavity dispersion and mode-locked pulse intensity, shorter pulses could be generated directly from Yb^{3+}-doped mode-locked $GdScO_3$ lasers. All the results indicate that Yb:$GdScO_3$ crystal are prospective for achieving few-optical-cycle pulse generation around 1 μm.

Funding. National Natural Science Foundation of China (61975071).

Optics EXPRESS

Disclosures. The authors declare no conflicts of interest.

Data availability. Data underlying the results presented in this paper are not publicly available.

References

1. X. M. Chen, L. Xu, H. Hu, *et al.*, "High-efficiency, high-average-power, CW Yb:YAG zigzag slab master oscillator power amplifier at room temperature," Opt. Express **24**(21), 24517–24523 (2016).
2. C. G. Carlson, P. D. Dragic, R. K. Price, *et al.*, "A Narrow-Linewidth, Yb Fiber-Amplifier-Based Upper Atmospheric Doppler Temperature Lidar," IEEE J. Select. Topics Quantum Electron. **15**(2), 451–461 (2009).
3. Z. Wang, B. Liu, Q. Q. Sun, *et al.*, "Upconverted Metal-Organic Framework Janus Architecture for Near-Infrared and Ultrasound Co-Enhanced High Performance Tumor Therapy," ACS Nano **15**(7), 12342–12357 (2021).
4. S. Olmschenk, D. N. Matsukevich, P. Maunz, *et al.*, "Quantum Teleportation Between Distant Matter Qubits," Science **323**(5913), 486–489 (2009).
5. R. Gaume, B. Viana, J. Derouet, *et al.*, "Spectroscopic properties of Yb-doped scandium based compounds $Yb:CaSc_2O_4$, $Yb:SrSc_2O_4$ and $Yb:SC_2SiO_5$," Opt. Mater. **22**(2), 107–115 (2003).
6. G. Boulon, Y. Guyot, H. Canibano, *et al.*, "Characterization and comparison of Yb^{3+}-doped $YA1O_3$ perovskite crystals (Yb : YAP) with Yb^{3+}-doped $Y_3Al_5O_{12}$ garnet crystals (Yb : YAG) for laser application," J. Opt. Soc. Am. B **25**(5), 884–896 (2008).
7. W. D. Tan, D. Y. Tang, X. D. Xu, *et al.*, "Room temperature diode-pumped $Yb:CaYAIO_4$ laser with near quantum limit slope efficiency," Laser Phys. Lett. **8**(3), 193–196 (2011).
8. S. D. Uemura and K. J. Torizuka, "Sub-40-fs Pulses from a Diode-Pumped Kerr-Lens Mode-Locked Yb-Doped Yttrium Aluminum Garnet Laser," Jpn. J. Appl. Phys. **50**(1R), 010201 (2011).
9. C. Paradis, N. Modsching, C. Krankel, *et al.*, "Generation of 35-fs pulses from a Kerr lens mode locked $Yb:Lu_2O_3$ thin-disk laser," Opt. Express **25**(13), 14918–14925 (2017).
10. W. T. Tian, Y. N. Peng, Z. J. Yu, *et al.*, "Diode-pumped power scalable Kerr-lens mode-locked Yb:CYA laser," Opt. Express **26**(5), 5962–5969 (2018).
11. J. Ma, Y. Fan, W. L. Gao, *et al.*, "Sub-five-optical cycle pulse generation from a Kerr-lens mode-locked $Yb:CaYAlO_4$ laser," Opt. Lett. **46**(10), 2328–2331 (2021).
12. Z. L. Lin, W. Z. Xue, X. D. Xu, *et al.*, "Semiconductor saturable absorber mirror mode-locked Yb:YAP laser," Opt. Express **30**(18), 31986 (2022).
13. W. D. Chen, Z. L. Lin, H. J. Zeng, *et al.*, "Sub-30 fs Kerr-lens mode-locked $Yb:SrLaAlO_4$ laser," IEEE Ind. Electron. **1**(2), SF2N.1 (2023).
14. R. Uecker, H. Wilke, D. G. Schlom, *et al.*, "Spiral formation during Czochralski growth of rare-earth scandates," J. Cryst. Growth **295**(1), 84–91 (2006).
15. B. Veličkov, V. Kahlenberg, R. Bertram, *et al.*, "Crystal chemistry of $GdScO_3$, $DyScO_3$, $SmScO_3$ and $NdScO_3$," Z. Kristallogr. **222**(9), 466–473 (2007).
16. W. T. Hou, H. Y. Zhao, Z. P. Qin, *et al.*, "Spectroscopic and continuous-wave laser properties of $Er:GdScO_3$ crystal at 2.7 μm," Opt. Mater. Express **10**(11), 2730 (2020).
17. Q. S. Song, N. Zhang, J. Liu, *et al.*, "Efficient continuous wave and broad tunable lasers with the $Tm:GdScO_3$ crystal," Opt. Lett. **48**(3), 640–643 (2023).
18. N. Zhang, Q. S. Song, J. J. Zhou, *et al.*, "44-fs pulse generation at 2.05 μm from a SESAM mode-locked $Tm:GdScO_3$ laser," Opt. Lett. **48**(2), 510–513 (2023).
19. Y. H. Zhang, C. H. Huang, M. Xu, *et al.*, "$Nd:GdScO_3$ crystal: Polarized spectroscopic, thermal properties, and laser performance at 1.08 μm," Opt. Laser Technol. **167**, 109709 (2023).
20. Y. H. Zhang, S. M. Li, X. Du, *et al.*, "$Yb:GdScO_3$ crystal for efficient ultrashort pulse lasers," Opt. Lett. **46**(15), 3641–3644 (2021).
21. P. Arsenev, K. Bienert, and R. Sviridova, "Spectral properties of neodymium ions in the lattice of $GdScO_3$ crystals," Phys. Stat. Sol. (a) **9**(2), K103–K104 (1972).
22. Y. Cheng, X. Xu, X. B. Yang, *et al.*, "Crystal growth, optical properties, and laser operation of Yb^{3+}-doped NYW single crystal," Laser Phys. **19**(11), 2133–2139 (2009).
23. F. Peng, W. P. Liu, Q. L. Zhang, *et al.*, "Growth, structure, and spectroscopic characteristics of a promising yellow laser crystal $Dy:GdScO_3$," J. Lumin. **201**, 176–181 (2018).
24. M. Siebold, S. Bock, U. Schramm, *et al.*, "$Yb:CaF_2$ — a new old laser crystal," Appl. Phys. B: Lasers Opt. **97**(2), 327–338 (2009).
25. X. D. Wang, X. D. Xu, Z. W. Zhao, *et al.*, "Comparison of fluorescence spectra of $Yb:Y_3Al_5O_{12}$ and $Yb:YAlO_3$ single crystals," Opt. Mater. **29**(12), 1662–1666 (2007).
26. D. Z. Li, X. D. Xu, Y. Cheng, *et al.*, "Crystal growth and spectroscopic properties of $Yb:CaYAlO_4$ single crystal," J. Cryst. Growth **312**(14), 2117–2121 (2010).
27. A. Schmidt, V. Petrov, U. Griebner, *et al.*, "Diode-pumped mode-locked $Yb:LuScO_3$ single crystal laser with 74 fs pulse duration," Opt. Lett. **35**(4), 511–513 (2010).
28. K. Beil, C. J. Saraceno, C. Schriber, *et al.*, "Yb-doped mixed sesquioxides for ultrashort pulse generation in the thin disk laser setup," Appl. Phys. B **113**(1), 13–18 (2013).
29. S. Kalusniak, A. Uvarova, I. Arlt, *et al.*, "Growth, characterization, and efficient laser operation of Czochralski- and micro-pulling-down-grown Yb^{3+}:$YScO_3$ mixed sesquioxides," Opt. Mater. Express **14**(2), 304–318 (2024).

Optics EXPRESS

30. J. H. Liu, Y. Wan, Z. C. Zhou, *et al.*, "Comparative study on the laser performance of two Yb-doped disordered garnet crystals: Yb:CNGG and Yb:CLNGG," Appl. Phys. B **109**(2), 183–188 (2012).
31. F. F. Liu, L. Dong, J. X. Chen, *et al.*, "Spectroscopic and lasing properties of a mixed (Yb, Y, Lu, Gd) calcium oxyborate crystal: $Yb_{0.19}Y_{0.34}Lu_{0.12}Gd_{0.35}Ca_4O(BO_3)_3$," J. Lumin. **232**, 117789 (2021).
32. S. X. Wang, K. Wu, Y. C. Wang, *et al.*, "Spectral and lasing investigations of Yb:YSGG crystal," Opt. Express **21**(14), 16305–16310 (2013).